Social Cognitive and Affective Neuroscience, 2018, 819–830

doi: 10.1093/scan/nsy064
Advance Access Publication Date: 22 August 2018
Original article

Functional connectivity in the social brain across childhood and adolescence

Ethan M. McCormick,† Jorien van Hoorn,† Jessica R. Cohen, and Eva H. Telzer

Department of Psychology and Neuroscience, University of North Carolina, Chapel Hill, North Carolina 27599, USA

Correspondence should be addressed to Eva H. Telzer, 235 E. Cameron Avenue Chapel Hill, NC 27514, USA. Email: ehtelzer@unc.edu.
†denotes equal authorship

Abstract

Previous research has characterized a collection of neural regions which support social-cognitive processes. While this 'social brain' is often described as a cohesive unit, it has been largely assessed with univariate methodologies, which cannot account for functional relationships 'between' brain regions, and therefore cannot test the idea of the social brain as a network. In the present work, we utilized a multi-method approach to empirically assess the functional architecture of the social brain. Fifty participants (ages 8–16) completed a social evaluation task during an functional imaging scan. Results from three unique functional connectivity methodologies demonstrated that social brain regions show strong functional relationships, while also interfacing with non-social regions, suggesting that future work should consider network relationships between social brain regions in addition to traditional univariate approaches. We probed, but did not find age-related differences in social brain network organization, demonstrating that this functional architecture is in place by late childhood.

Key words: social brain; network; PPI; graph theory; ICA

Introduction

'Man is by nature a social animal' (Aristotle, translated 1944). The capacity to understand the social world is supported by a collection of brain regions often referred to as the social brain (Brothers, 1990; Saxe, 2006; Dunbar and Shultz, 2007; Frith and Frith, 2007; Lieberman, 2007; Adolphs, 2009; van Overwalle, 2009). There has been a surge in work examining the developmental properties of the social brain, as structural and functional brain development parallels dynamic changes in social orientation during late childhood and adolescence (Nelson *et al.*, 2005; 2016; Blakemore, 2008; Blakemore and Mills, 2014; Mills *et al.*, 2014). Strikingly, the social brain is often described as a cohesive entity, or network, despite most research utilizing univariate, activity-based approaches that do not explicitly measure connections amongst social brain regions. In order to determine whether social brain regions act as a cohesive network, it is critical to measure such connections. In addition to determining whether the social brain acts as a network, it is important to determine whether and how the network properties of the social brain change during the transition between childhood and adolescence. In the present work, we employed a multi-method network approach to test the functional architecture of the putative social brain network.

Social cognition enables individuals to recognize others and evaluate their thoughts and feelings (i.e. mentalizing). A model of the social brain (Blakemore, 2008; Blakemore and Mills, 2014) in developmental neuroscience implicates amygdala, anterior insula (AI), superior temporal sulcus (STS) and prefrontal cortex (PFC) in the recognition of others' emotions, and the temporo-parietal junction (TPJ), anterior temporal poles (TP)

Received: 18 April 2018; **Revised:** 4 July 2018; **Accepted:** 24 July 2018

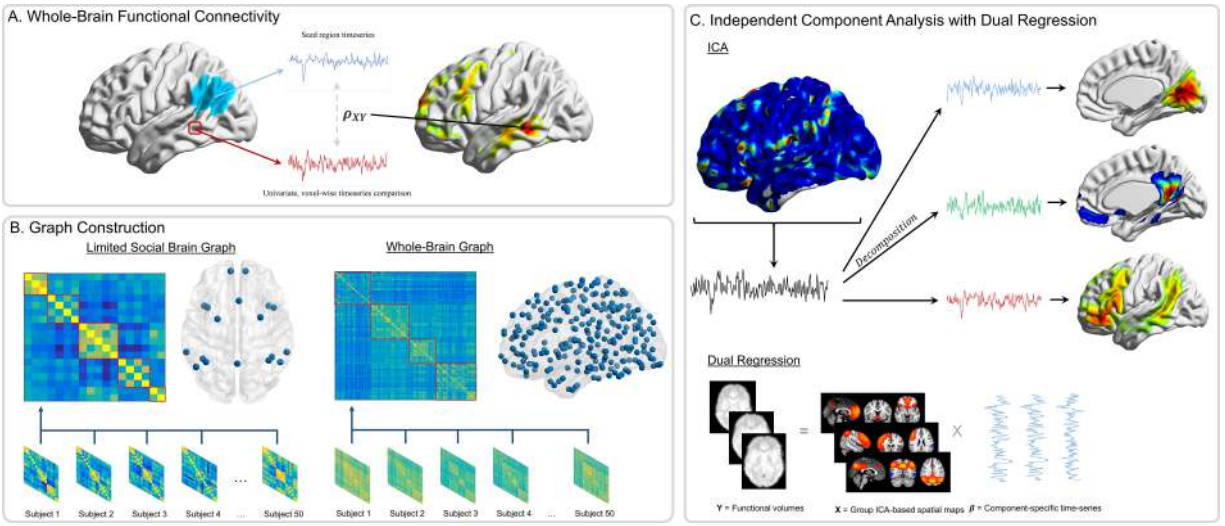

Fig. 1. Functional connectivity approaches. (A) Whole-brain functional connectivity utilizing PPI is a voxel-wise method. The average time-series is extracted from the seed region (blue), and then time-series from each voxel (e.g. red) are compared using time-series correlations (ρ_{XY}). These correlation values are mapped onto the whole-brain statistic map. (B) Graph construction involves calculating time-series correlations between each pair of nodes (either 18 or 282) to construct individual subject correlation matrices. Individual matrices are then averaged together and community detection algorithms are applied to the group-level matrices to group nodes into functional networks (indicated by red boxes). (C) ICA utilizes multivariate mixture modeling in order to group voxel time-series into functional units. Time-series from all voxels in the brain are added to the mixture model and then decomposed into spatial maps of voxels which have similar time-series features. These group-level maps (**X**) are then used in the Dual Regression analyses to extract component-specific time-series ($\boldsymbol{\beta}$) from each individual's functional volumes (**Y**).

and the medial PFC to be involved in mentalizing. Although it remains contested whether the social brain is uniquely devoted to social cognition (e.g. Decety and Lamm, 2007), previous developmental work employing univariate methodologies consistently supports the recruitment of social brain regions in tasks that require social cognition from childhood into adulthood (e.g. Blakemore *et al.*, 2007; Burnett *et al.*, 2009; van den Bos *et al.*, 2011; Gweon *et al.*, 2012; Schurz *et al.*, 2014; van Hoorn *et al.*, 2016).

Despite these univariate findings, oftentimes not 'all' regions implicated in specific social cognition processes, such as mentalizing, are engaged together even during tasks that specifically implicate mentalizing (e.g. reciprocity, TPJ only [van den Bos *et al.*, 2011]; being observed by peers, mPFC only [Somerville *et al.*, 2013]), which questions the individual contributions of each region within the larger social brain network. More recent advances have started to investigate functional connectivity between social brain regions and affective or cognitive control regions (e.g. mPFC–ventral striatum; Somerville *et al.*, 2013; Qu *et al.*, 2015). However, to date, social brain regions have not often been utilized as a seed region, and as such, connections 'between' regions of the putative social brain network have largely been absent from the literature (but see Burnett and Blakemore, 2009). Furthermore, no previous studies have considered multiple functional relationships between systems of social brain regions simultaneously. Hence, taking a network approach will allow us to make more specific predictions and increase our understanding of the role of each social brain region within the larger network.

In the present work, we utilized both theory- and data-driven techniques to gain traction on the functional architecture of the social brain network. During an fMRI scan, children and adolescents (ages 8–16) completed a social evaluation task, a context in which we expected the social brain to be particularly engaged (van Hoorn *et al.*, 2016). We first used seed-based PPI, which assessed the whole-brain functional connectivity profiles for all a priori social brain regions of interest (Blakemore, 2008; Blakemore and Mills, 2014). This approach allowed us to independently examine functional relationships with each theoretically derived region. Next, in order to assess the pattern of functional relationships between all regions of the social brain simultaneously, we adopted a graph theory approach which mapped the overall structure of the proposed network. Finally, we took an entirely data-driven approach to examine if the social brain network could be resolved through automated multivariate mixture-modeling of the time-series using independent and principle components analysis (see Figure 1 for summary). This data-driven approach allowed us to be more confident that results were not biased by decisions of which seed regions to use or the particular morphology of any given a priori region of interest (ROI). In each of these analyses, we tested for potential linear and curvilinear developmental changes in the functional architecture of the social brain network, given previous evidence that activation in social brain regions changes across development (e.g. Blakemore *et al.*, 2007; Burnett *et al.*, 2009; van den Bos *et al.*, 2011; Gweon *et al.*, 2012; van Hoorn *et al.*, 2016; reviewed in Blakemore and Mills, 2014; Nelson *et al.*, 2016). Together, our multi-method approach leveraged the different strengths of each type of analysis to provide a comprehensive assessment of the social brain's functional architecture.

Methods

Participants

Fifty-one children and adolescents completed an fMRI scan. One participant was excluded due to moving out of the field of view, leaving a final sample of fifty youths (M_{age} = 13.51 years, SD = 2.66, *range* = 8.31–16.45; 29 males). Inclusion in the final sample required less than 2 mm framewise displacement motion on 90% of volumes, however, no further participants were excluded based on this criterion. Participants provided written assent, and parents provided written consent in accordance with the University's Institutional Review Board.

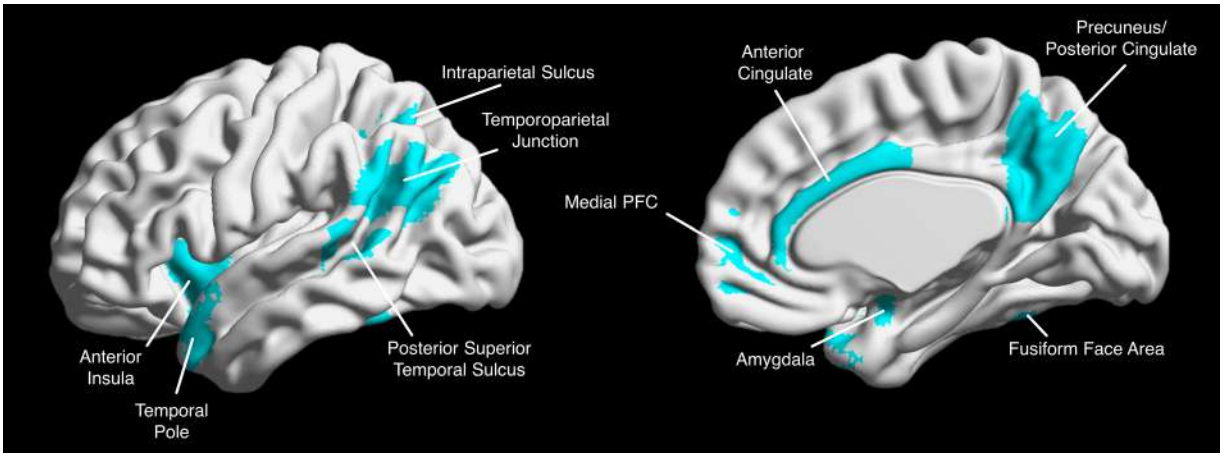

Fig. 2. Social brain regions of interest. We constructed 18 independent ROIs for each of the putative social brain regions. ROIs were combined into one map for visualization.

Social evaluation task

During the scan session, participants completed a social evaluation task in which they were asked to consider others' thoughts about themselves. Previous research has shown a univariate signature of the social brain during tasks in which adolescents receive social evaluation (e.g. Pfeifer *et al.*, 2009; Somerville, 2013; van Hoorn *et al.*, 2016). As such, we chose this task to maximize the likelihood of observing connectivity between social brain regions. In other words, if regions of the social brain do not operate as a network under these conditions, they would be unlikely to do so under other, less salient social contexts. Adolescents and children saw a series of 72 peer faces (ranging in age from 7–17 years; all smiling) and were asked to judge whether they thought each peer would like or dislike them by pressing one of two buttons for 'Like' and 'Dislike'. Aside from asking participants to judge whether the person depicted in a given stimulus would 'Like' or 'Dislike' them, participants were not given information about the identity or characteristics of the individuals depicted, and participants received no feedback based on their choices. Faces were drawn from several databases, including the National Institute of Mental Health Child Emotional Faces Picture Set (Egger *et al.*, 2011) and had of equal numbers of males and females. Each face was presented for 3 s each, in random order, with a gamma-distributed inter-trial jitter ($M_{duration}$ = 2 s). Consistent with similar tasks used previously, the main effect of the social evaluation task showed increased activation in several social brain regions, as well as in lateral PFC and ventral striatum (see NeuroVault: https://neurovault.org/collections/FAPLBMIG/ for statistical map; see Supplementary Material for methods).

fMRI data acquisition

Imaging data were collected using a 3 Tesla Siemens Trio MRI scanner. The Social Evaluation Task included T2*-weighted echoplanar images (EPI; 185 volumes; slice thickness = 3 mm; 38 slices; TR = 2 s; TE = 25 msec; matrix = 92 × 92; FOV = 230 mm; voxel size 2.5 × 2.5 × 3mm^3). In addition, structural scans consisted of a T2*weighted, matched-bandwidth (MBW), high-resolution, anatomical scan (TR = 4sec; TE = 64 msec; FOV = 230; matrix = 192 × 192; slice thickness = 3 mm; 38 slices) and a T1* magnetization-prepared rapid-acquisition gradient echo (MPRAGE; TR = 1.9 s; TE = 2.3 msec; FOV = 230; matrix = 256 × 256; sagittal plane; slice thickness = 1 mm; 192 slices). To maximize brain coverage, MBW and EPI scans were obtained using an oblique axial orientation.

Preprocessing was completed using FSL FMRIBs Software Library (FSL v6.0; https://fsl.fmrib.ox.ac.uk/fsl/). Preprocessing steps included the following: correction for slice-to-slice head motion using the MCFLIRT; spatial smoothing using a 6 mm Gaussian kernel, full-width-at-half maximum; high-pass temporal filtering with a 128 s cutoff to remove low frequency drift across the time-series; and skull stripping of all images with BET. Functional images were re-sampled to a 2 × 2 × 2 mm space and co-registered sequentially to the MBW and the MPRAGE using FLIRT in order to warp them into the standard stereotactic space defined by the Montreal Neurological Institute and the International Consortium for Brain Mapping. Individual-level independent component analysis (ICA) using MELODIC combined with an automated component classifier (Tohka *et al.*, 2008; Neyman–Pearson threshold = 0.3) was applied to remove artifact signal (e.g. motion, physiological noise).

The Social Evaluation Task was modeled using a block design within the Statistical Parametric Mapping software package (SPM8; Wellcome Department of Cognitive Neurology, Institute of Neurology, London, UK). Each block was modeled using a fixed onset of 4 s after the first slice acquisition and a duration of 362 s (i.e. the remainder of the functional scan). Fixed-effects models were created by including a general linear model for the task. Volumes containing motion in excess of 2 mm slice-to-slice were modeled in a separate regressor of no interest. All participants in the final sample showed less than 2 mm of framewise displacement for over 95% of total volumes.

Analytic approaches

ROI definition. In order to assess the social brain network, we utilized pre-defined ROIs within the putative social brain network, based on a theoretical model of the social brain (Blakemore 2008; Blakemore and Mills, 2014). These ROIs included bilateral masks of the TPJ, pSTS, IPS, TP, AI, amygdala, FFA, mPFC, as well as masks of the ACC and precuneus (see Figure 2). Masks were defined from a number of sources, including the Harvard–Oxford (ACC, AI, amygdala; Harvard Center for Morphometric Analysis) and SPM Anatomy toolbox (IPS, TP, FFA; Eickhoff *et al.*, 2005) probabilistic atlases, the Saxe Lab social brain ROIs (TPJ, precuneus; Dufour *et al.*, 2013) and

the social brain ROIs defined by Mills *et al.* (2014; mPFC, pSTS). The mPFC in particular refers to an area of medial frontal cortex anterior to the cingulate cortex, extending primarily through medial sections of BA11. Masks were evaluated using the Marsbar toolbox in SPM (Brett *et al.*, 2002) in order to ensure that ROIs did not contain any voxels that overlapped with another mask. A 3D, navigable image containing all masks superimposed onto a single brain map is available on NeuroVault (https://neurovault.org/collections/FAPLBMIG/).

Whole-brain functional connectivity analyses. First, to examine neural connectivity in the social brain at the whole-brain level, we employed psychophysiological interaction (PPI) analyses. Importantly, PPI analyses were run separately for each ROI, resulting in 18 independent iterations for each type of analysis (detailed below). Prior to running analyses, we inspected individual subjects' whole-brain mask to ensure that all included subjects had at least 90% coverage for each of the 18 ROI masks. We utilized a generalized form of the context-dependent PPI analyses from the automated generalized PPI (gPPI) toolbox in SPM (McLaren *et al.*, 2012), in which deconvolved time-series were extracted from each of the 18 ROI masks for each participant to create the physiological variables. Psychological regressors were created by convolving each participants' block contrast, which was constructed as a single regressor spanning the entire task duration (duration = 361 s), with canonical HRFs. PPI interaction terms were created by multiplying the physiological variable with the psychological regressor. This interaction term was applied at the whole-brain level to identify regions that covary across the block with the seed ROI (Figure 1A). Regressors computed for each participant represented the deconvolved BOLD signal, and this regressor was included alongside each psychological and PPI term for the block event to create a gPPI model. Random effects, group-level analyses were run for all contrasts using GLMFlex (http://mrtools.mgh.harvard.edu/index.php/GLM_Flex), which offers several advantages, including removing outliers and sudden activation changes in brain, correcting for variance–covariance inequality, partitioning error terms and analyzing all voxels containing data. Main-effect, one-sample *t*-tests were run for each of the 18 ROI seed regions to assess the whole-brain pattern of functional connectivity for each seed region. In order to examine whether connectivity within the social brain changes across development, group-level regression analyses were also performed for all 18 ROI seed regions by entering participants' age as a continuous covariate in whole-brain regression analyses. To assess for higher-order age effects, we also entered age^2 as a continuous predictor in a whole-brain regression analysis, controlling for linear age.

Given the large number of independent analyses, we applied a two-step correction for multiple comparisons in our whole-brain PPI analyses in order to control for an inflated Type I error rate. First, for each individual analysis (e.g. main effect or regression), we utilized the voxel-level correction estimated through the SPM software package, which resulted in a voxel-wise threshold of ($P = 9.82 \times 10^{-7}$, $t = 5.40$). However, because we ran 18 independent tests each for the main effect and both age and age^2 regression analyses (54 total analyses), we also applied a Bonferroni correction for multiple significance tests (i.e. $\alpha_{adjusted} = \alpha_{unadjusted}/54$). These steps resulted in a final voxel-wise threshold of $P = 1.82 \times 10^{-8}$ ($t = 6.52$). All reported effects and inferences are based on this corrected threshold, and unthresholded maps are available on NeuroVault (https://neurovault.org/collections/FAPLBMIG/).

Finally, we created a composite map of the PPI analyses across all 18 social brain seed regions. Importantly, this composite was not intended as a formal, independent analysis, but rather a convenient and succinct tool for summarizing findings across the many independent analyses we conducted. We created this map by averaging the t-statistics for connectivity values for each voxel in the whole-brain mask across the 18 main effect analyses. As such, larger values in the composite map suggest that a given region is more strongly coactive consistently across different social brain seeds, while smaller values suggest a low average co-activation with the social brain. For descriptive purposes, we applied the same corrected threshold parameters used in the analyses described above for the composite map and this composite map is similarly available on NeuroVault.

Graph construction. Second, we utilized graph theory techniques to investigate the functional network structure of the social brain. In order to construct a time-series for each ROI, we utilized a beta-series correlation approach (Rissman *et al.*, 2004). For all participants, we estimated the magnitude of the task-related BOLD response separately for each of the 72 trials during the task; modeled as the activity evoked from stimulus onset to the button press indicating participants' choice. This approach yields a set of parameter estimates (beta values) for each trial in every voxel across the whole-brain. These beta values can then be concatenated to form a time-series, known as a beta-series. Beta-series were extracted from each ROI and individual correlation matrices were constructed by computing time-series correlations between each pair of nodes for each participant. Each participant's beta-series was reviewed to ensure that no ROIs were subject to signal dropout, and all 50 included participants had at least 90% coverage in all ROIs. Graphs were created using connectivity matrices and tools from MATLAB (MathWorks; https://www.mathworks.com) and the Brain Connectivity Toolbox (www.brain-connectivity-toolbox.net; Rubinov and Sporns, 2010).

We took two approaches to evaluate the graph network structure of the social brain. First, we assessed the functional relationships amongst theoretical nodes of the social brain in isolation. Next, we evaluated the network organization of social brain regions in the context of the larger functional architecture of the whole brain. The steps we took to construct functional network graphs were identical across both approaches, with the one exception that for the first approach, we used 18-node correlation matrices to construct graphs, whereas for the second approach, we utilized a whole-brain parcellation to construct 282-node correlation matrices. We used the Power parcellation scheme (Power *et al.*, 2011), a 264-node atlas composed of 10 mm spherical parcels distributed throughout the entire brain. To make our ROIs more compatible with this atlas, we constructed 10 mm sphere versions of each of our 18 social brain masks located at the center-of-gravity coordinates for individual ROIs. Similar to the full ROIs previously described, a 3D, navigable image of these spherical ROIs is available on NeuroVault (https://neurovault.org/collections/FAPLBMIG/). Whole-brain network analyses were run using both full and 10 mm sphere versions of the social brain ROIs to ensure that results were not dependent on the type of ROI used (i.e. full versus sphere). As results were consistent across both types of ROIs, we report analyses using the 10 mm sphere versions of our social brain ROIs since they are consistent with the other parcels in the Power atlas. For details related to graph construction and community clustering, see supplement (Supplementary pp. 1–2).

Network building and community clustering techniques. In order to structure our correlation matrices, we first clustered nodes within the larger network into functionally integrated and distinct communities. For each participant, nodes within the putative social brain network were assigned to communities within the network using consensus clustering techniques (Lancichinetti and Fortunato, 2012). Weighted edges (both positive and negative) from the unthresholded correlation matrices for each participant were passed through the Louvain community detection algorithm, which assigned each node into a larger community (Rubinov and Sporns, 2011) using a resolution parameter (γ) of 1.25, based on previous research (Power *et al.*, 2011; Cohen and D'Esposito, 2016). Due to the stochastic nature of the Louvain algorithm, community detection was iterated 150 times, and all derivations were passed into an agreement matrix ($D_{i,j}$) where each cell (i,j) within the matrix indicated the proportion of iterations in which each pair of nodes were assigned to the same community. Agreement matrices were then thresholded at 0.5 to remove spurious or accidental assignment of nodes to the same community. As such, nodes that were not assigned to the same community in at least 50% of the community detection algorithm iterations were set to 0. A consensus partition for each participant was created by applying the Louvain algorithm 100 times for the participants' agreement matrix ($D_{i,j}$). Once consensus partitions had been created for each individual participant, we created a group consensus partition by creating a group agreement matrix (D) using the community assignments from individuals for each node pair. This matrix was then divided by the number of participants in our sample such that each cell within the group agreement matrix represented the proportion of individuals in which a given node pair was assigned to the same community. Finally, to compute a group network structure, this group agreement matrix was passed into the consensus clustering algorithm and iterated 1000 times until it converged on an optimal community structure.

For both approaches, we examined whether there was a significant relationship between age and the weight of each functional edge. As results indicated no significant effect of age (see Results for more detail), we collapsed across all participants to construct the group-level correlation matrix by averaging participants' weight for each edge. Group-level correlation matrices were created for both the 18- and 282-node graphs, and nodes were reordered to reflect the optimal community structure determined previously (visualized by red boundaries within the group correlation matrices, Figure 1B). Finally, graphs were thresholded in order to remove the effects of weak or spurious connections between node pairs. Consistent with previous research, we thresholded graphs at a range of costs (10–25% of total edges, 5% increments) to ensure that results were not due to chance perturbations at any one cost. These thresholds have been previously shown to produce graphs with small-world characteristics (Bullmore and Bassett, 2011; Cohen and D'Esposito, 2016). Because of the relatively small number of nodes in the 18-node analysis, we also explored costs from 25–35% (5% increments) as well for this approach specifically. Reported results for network statistics are averaged across all costs, however, for visualization purposes, we display graphs at both a strict (10%) and a liberal (35% for 18-node graph; 25% for 282-node graph) threshold.

Graph metrics. We also calculated network-level variables for each individual using their functional correlation matrix. All graph metrics for individual-level networks were computed using tools in MATLAB and the Brain Connectivity Toolbox. We calculated network modularity, system segregation and global efficiency (for details, see supplementary).

ICA. Third, we utilized group-level ICA to assess whether similarities in the time-series of social brain regions could be assessed using a model-free, multivariate analytic approach. To do so, we pooled fMRI data from all 50 participants and ran temporally concatenated ICA with probabilistic principle component analysis (PCA; Beckmann and Smith, 2004; Beckmann *et al.*, 2009) using MELODIC's Incremental Group-PCA (MIGP) option for data reduction through FSL. This resulted in 40 independent components (see Supplementary or NeuroVault for visualization of all 40 components) on the whole functional time-series for the task. Group spatial maps were then examined visually to check for components that were likely due to physiological noise (e.g. motion or cardiovascular activity). These components (N = 16) were characterized by activation in white matter, ventricles or as slabs or bands of activation around the outer rim of the brain (see Laird *et al.*, 2011 for examples; noise components noted in Supplementary). We then took the group spatial maps generated in the ICA analysis and used the spatial regression approach from FSL's dual regression function (Filippini *et al.*, 2009) to extract individual time-series from each of the group-level masks, resulting in 24 time-series for each participant. These time-series were used to create 24 × 24 correlation matrices for each participant. We then ran community detection and group-level analyses on the resulting correlation matrices using the methods described in detail in the supplement for graph construction (Supplementary pp. 1–2).

Motion. Because functional connectivity methods (including graph construction and ICA) are particularly sensitive to motion during scan acquisition (e.g. Power *et al.*, 2012; Van Dijk *et al.*, 2012), we took several steps to reduce the impact of motion on our data. First, as mentioned above, we subjected each participants' data to individual-level ICA in order to remove motion-related signal from the time-series (mean framewise displacement: *M* = 0.27 mm; *range* = 0.03–1.47 mm). We also controlled for the 6 motion parameters generated during the realignment step of preprocessing in all analyses. Finally, slices with greater than 2 mm of motion were scrubbed from the time-series to remove the effects of large, sudden movements on the functional data. These strategies have been shown to reduce the influence of motion on functional connectivity analyses (see Ciric *et al.*, 2017).

Results

Whole-brain PPI

We began our examination of the putative social brain by utilizing seed-based connectivity analyses. We used each of the 18 a priori ROIs as seed regions in individual PPI analyses. This approach allowed us to examine the whole-brain functional relationships of each seed region independently.

Main effects. First, we ran whole-brain, one-sample *t*-test analyses for each of the 18 a priori social brain seed regions (for individual maps see Supplementary Tables S1–S18). While there was variation in the distribution of co-activation between seed regions, several consistent trends emerged. First, there were strong functional relationships between bilateral complements (e.g. left and right TPJ), suggesting that information

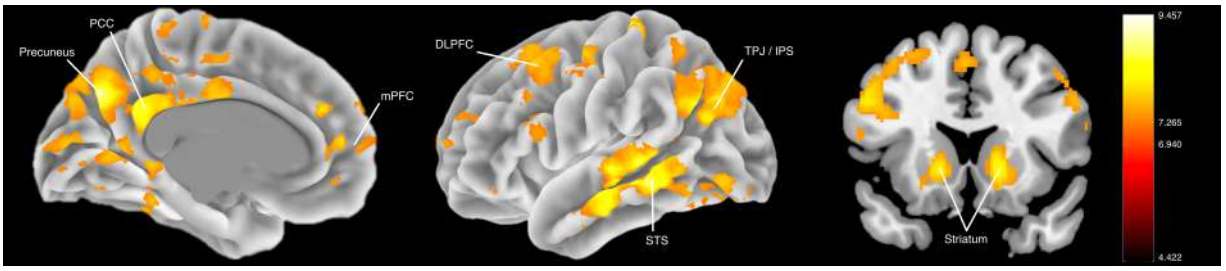

Fig. 3. Composite PPI map. Regions showing heightened parameter statistics suggest that those regions are consistently co-activated with social brain ROIs across the 18 main-effect PPI analyses.

is highly shared between contralateral homologs during social processing. Secondly, while there certainly was strong functional connectivity between seed regions and other social brain areas, these co-activations were often non-specific, as other regions of the brain (e.g. lateral PFC, striatum) were similarly co-active with many of the a priori seed regions. To quantify this overlap in functional connectivity between regions, we constructed a follow-up descriptive map where we summed t-statistics from the individual seed maps (excluding the seed region for each respective analysis) and scaled the values by dividing the summed t-statistics by the number of seed regions (i.e. 18). This averaging approach allowed us to visualize which regions at the whole-brain level are consistently co-active with the different seed regions from the social brain. Regions which showed the highest level of overlap in co-activation across seed regions included the thalamus and striatum, dorsal portions of the mPFC, PCC/precuneus, middle temporal gyrus, bilateral angular gyrus and regions of the middle and inferior frontal gyri (Figure 3; Supplementary Table S19 for full details).

Regressions with age. To examine developmental differences in the functional connectivity of social brain regions, we utilized a whole-brain regression approach for each seed region, entering age as a continuous regressor. When correcting for multiple comparisons, no seed region showed significant linear or quadratic developmental differences in co-activation at the whole-brain level. This suggests that by childhood, the functional network structure of the social brain may already be in place. Hence, we combined data from all subjects for subsequent analyses. In contrast, follow-up univariate analyses quantifying the main effect of the task showed some regional changes in activation with age (see Supplemental for regional effects).

Network analyses

Since both theoretical and empirical work has referred to the social brain as a network, we formally examined the functional relationships of putative social brain regions using a graph-theory network approach. In contrast to PPI analyses, where each seed region is considered independently, network analyses assess functional relationships between all included regions simultaneously, allowing us to assess an overall functional network structure to the social brain.

Limited social brain graph. We first extracted the beta-series from each of the 18 social brain seeds to construct individual correlation matrices and created a group-level matrix by averaging across all 50 participants. Data from this process were then used to construct a graph of the 18 social brain ROIs. Applying a strict threshold (e.g. 10%; Figure 4A) resulted in a fractured graph, with a temporo-parietal group of regions, an ACC/Insula group and bilateral pairs of regions otherwise (with FFA being the exception). However, we can see these groupings maintained in the full graph at more liberal thresholds (eg. 25%; Figure 4B), where temporo-parietal (purple) and temporo-limbic (orange) regions are linked by medial frontal regions (ACC & mPFC). Overall, these results suggest that while there may be component modules within the social brain, there are nevertheless important functional relationships linking these disparate regions.

Age analyses. While results from the PPI analyses suggested that there is limited development in the functional connectivity of social brain regions, we wanted to confirm that our graph model results were not being influenced by developmental effects. As such, we ran bivariate correlations between age and individual edge strength on the 35% threshold graph. Out of a total of 153 unique edges, only 10 (6.5%) showed age-associated change at uncorrected significance (i.e. $P < 0.05$), and only 5 (3.3%) showed significance at a more strict threshold (i.e. $P < 0.01$). When correcting for multiple comparisons, none of these correlations remained significant. We also conducted analyses to test for age-related change in network-level variables. Neither network modularity ($r = 0.15$, $P = 0.31$), system segregation ($r = 0.13$, $P = 0.37$), nor global efficiency ($r = -0.11$, $P = 0.46$) were related to age (see supplemental for definitions and equations). These results corroborate the whole-brain PPI regression analyses with age, suggesting that the social brain network does not differ across age and is relatively in place by childhood.

Whole-brain graph. Next, we examined the network relationships of the 18 social brain seeds with the rest of the brain utilizing the whole-brain parcellation provided by Power *et al.* (2011). We added the eighteen social brain ROIs (using 10 mm sphere versions, centered within the anatomical ROIs for consistency; see Methods for details) to the 264 spheres which comprise the Power parcellation scheme and constructed individual correlation matrices and ran the same graph-building procedure as above. Results extended findings from the limited social brain graph by demonstrating how these functional nodes are distributed throughout the whole-brain network. As expected, some functional subunits, such as the temporo-parietal (purple) and salience (green) nodes, show tightly integrated functional relationships, while other functional subunits, such as the mPFC, amygdala and TP (orange) are more marginalized from network centers (Figure 4C).

ICA

Finally, we wanted to ensure that our results were not being driven by choices or models we were imposing on the data. Therefore, we complemented our analyses with a data-driven

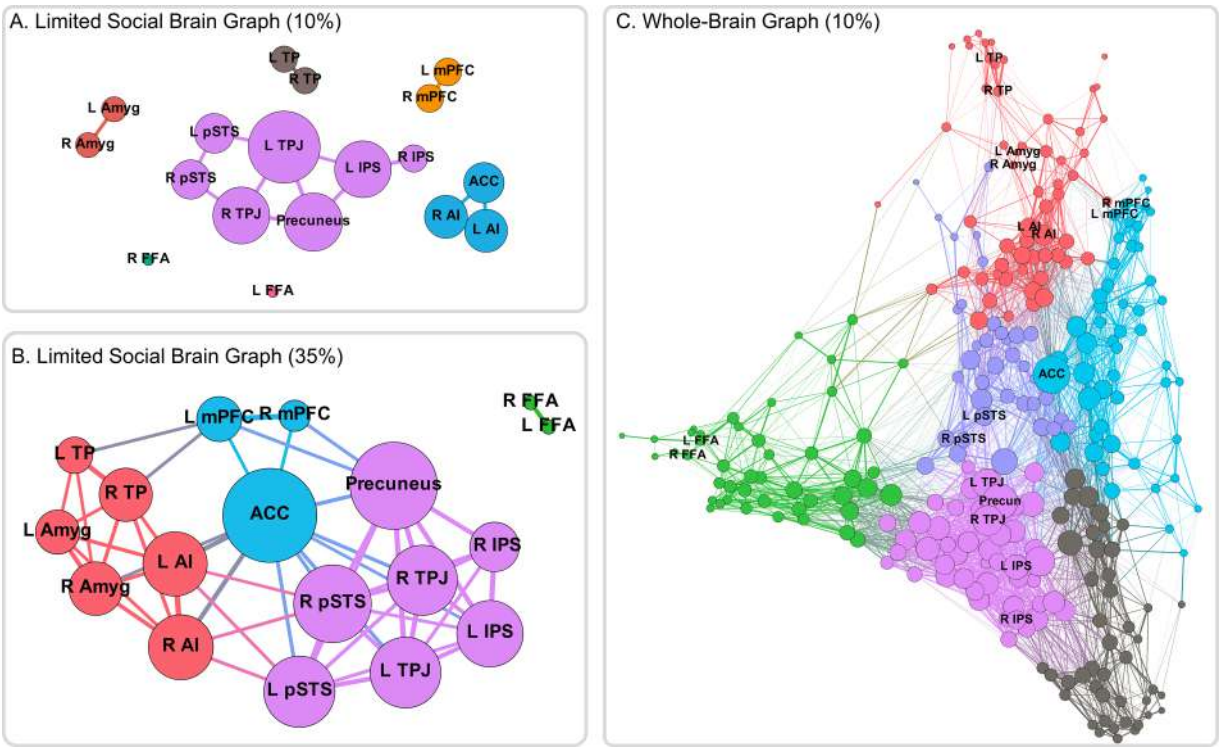

Fig. 4. Network graphs. (A) When thresholding the 18-node social brain graph at a strict threshold, the graph is fractured with only a temporo-parietal and a salience cluster linking disparate regions. (B) However, at a more liberal threshold, there appear to be three large clusters: a temporo-parietal cluster (purple), a temporo-limbic cluster (orange) and a midline frontal cluster (green) linking them. (C) Within the context of the larger, whole-brain network, regions of the social brain are distributed throughout network space. Some regions such as the temporo-parietal regions (purple) show strong, centralized connectivity patterns, whereas anterior temporal and amygdala regions (orange) are located on the margins of the network.

approach using ICA on the whole-brain data. Because ICA utilizes a multivariate approach to decompose spatial and temporal components from the raw functional data, it removes the necessity of specifying a model or parcellation scheme to structure the data a priori. As such, we could investigate whether regions of the social brain emerged as independent components from the data.

Whole-brain components. We ran whole-brain ICA using the automatic PCA option available in FSL's MELODIC (known as MIGP—MELODIC's Incremental Group-PCA; Smith *et al.*, 2014) to constrain the number of meaningful independent components. ICA resulted in 40 components (Figure 5), of which 24 were determined to be non-artefactual (for tables and maps for all components, see Supplementary Tables S20–S43 and NeuroVault, respectively; components determined to be noise artefacts are noted). We then used a dual regression approach to extract time-series information from each component's spatial maps in individual participants in order to run graph analyses. Using these individual time-series for the 24 independent components, we constructed individual and group correlation matrices and then used these matrices to perform community detection in order to find groups of components that were functionally related. We found four broad groups of components: (1) a four-component motor community; (2) a three-component cerebellar community; (3) a nine-component fronto-striatal community; and (4) an eight-component community that included three visual components and five social brain components (see Figure 6). Importantly, many regions of the social brain were strongly clustered together, supporting the idea that social brain regions share strong functional relationships.

Discussion

The concept of a social brain network has become prevalent in the developmental neuroscience literature, encompassing the neural structures that guide increasingly complex social cognition across development. Indeed, a growing body of work has revealed a collection of brain regions which are robustly active when thinking about or making decisions regarding others (Brothers, 1990; Saxe, 2006; Dunbar and Shultz, 2007; Frith and Frith, 2007; Lieberman, 2007; Adolphs, 2009; van Overwalle, 2009), and patterns of activation in these regions continue to be refined across late childhood and adolescence (e.g. Blakemore *et al.*, 2007; Burnett *et al.*, 2009; van den Bos *et al.*, 2011; Gweon *et al.*, 2012; Mills *et al.*, 2014; Van Hoorn *et al.*, 2016). However, previous methodologies used to probe the social brain have not evaluated the social brain as a 'network'. To gain traction on the network architecture of the social brain, the current work investigated the functional relationships between regions of the putative social brain network using seed-based connectivity, graph theory and ICA techniques. As these techniques varied in the amount of theoretical constraints imposed on the data, they complemented each other to ensure that results are not simply a product of modeling decisions particular to any one type of analysis. While regions of the social brain network do indeed show strong functional relationships between one another, these relationships are not exclusive and other regions emerged as important functional hubs. In contrast with findings showing protracted development in social brain regions through adolescence (e.g., Blakemore *et al.*, 2007; Burnett *et al.*, 2009; van den Bos *et al.*, 2011; Gweon *et al.*, 2012; Mills *et al.*, 2014; Van Hoorn *et al.*, 2016), results suggest that the underlying functional architecture of the social brain appears to be in

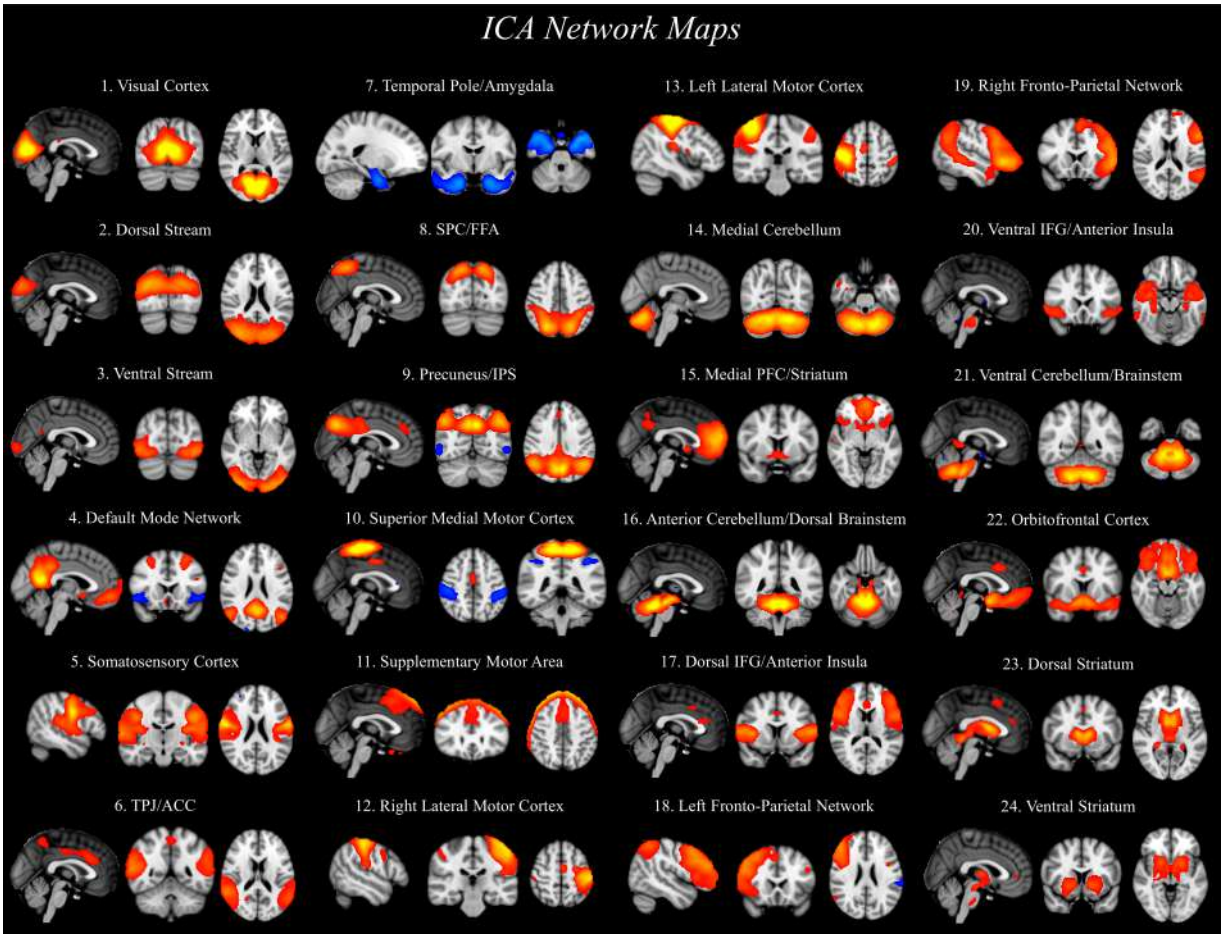

Fig. 5. Twenty-four independent components were decomposed through group-level ICA analysis. ICA maps were converted to z statistic images via normalized mixture model fit, thresholded at $z > 3.5$. Slices of the most representative extent of the spatial maps are shown. Components identified as noise are not presented, but are available for viewing on NeuroVault.

place relatively early in development. These findings highlight the importance of considering functional relationships in evaluating social cognition and embedding social-cognitive neural processes in the context of the larger brain circuitry.

Functional architecture of the social brain network

Our multi-method approach uncovered several features of the functional architecture of the social brain. PPI analyses revealed that when considering the functional connectivity patterns of each a priori seed region independently, other regions of the putative social brain network consistently emerged. This pattern can be seen in the robust co-activation of social brain regions in our composite map across the 18 independent analyses. These findings are corroborated by the ICA analyses, where data-derived components show that social brain seeds are grouped together. At the same time, our findings argue against the idea of the social brain being an exclusive network, but rather one that can integrate with other networks depending on task demands. All three methods employed here suggest that regions of the social brain are embedded within a larger functional architecture encompassing regions outside the social brain. The PPI analyses highlighted the striatum and lateral PFC as being consistently co-active with social brain seeds and the ICA network demonstrated that there are strong links between social brain components and regions of the fronto-striatal cluster.

While the specific regions showing strong co-activation are likely dependent on task demands, the current findings suggest that regions non-specific to social cognition nevertheless show high functional integration with social brain regions. Moreover, the limited and whole-brain graphs demonstrated that regions of the social brain are clustered into distinguishable modules, which are widely distributed throughout network space, indicating that the functional relationships between modules are relatively weak. For instance, regions of the temporo-parietal cluster (purple nodes, Figure 4C) are highly clustered in a relatively central part of the whole-brain graph, whereas regions such as the amygdala or temporal pole are peripheral in the whole-brain graph. These network positions are also reflected in the limited social brain graph, where, at strict thresholds, only the temporo-parietal and salience regions show links outside of bilateral counterparts. Taken together, given the complexity of social-cognitive processes, whole-brain graph approaches will likely provide more contextualized findings when assessing functional relationships between distributed regions in the brain than when restricting the nodes under consideration to social brain regions.

Developmental changes in the social brain network

Despite theoretical reasons to expect that the network of social brain regions would undergo functional changes across the

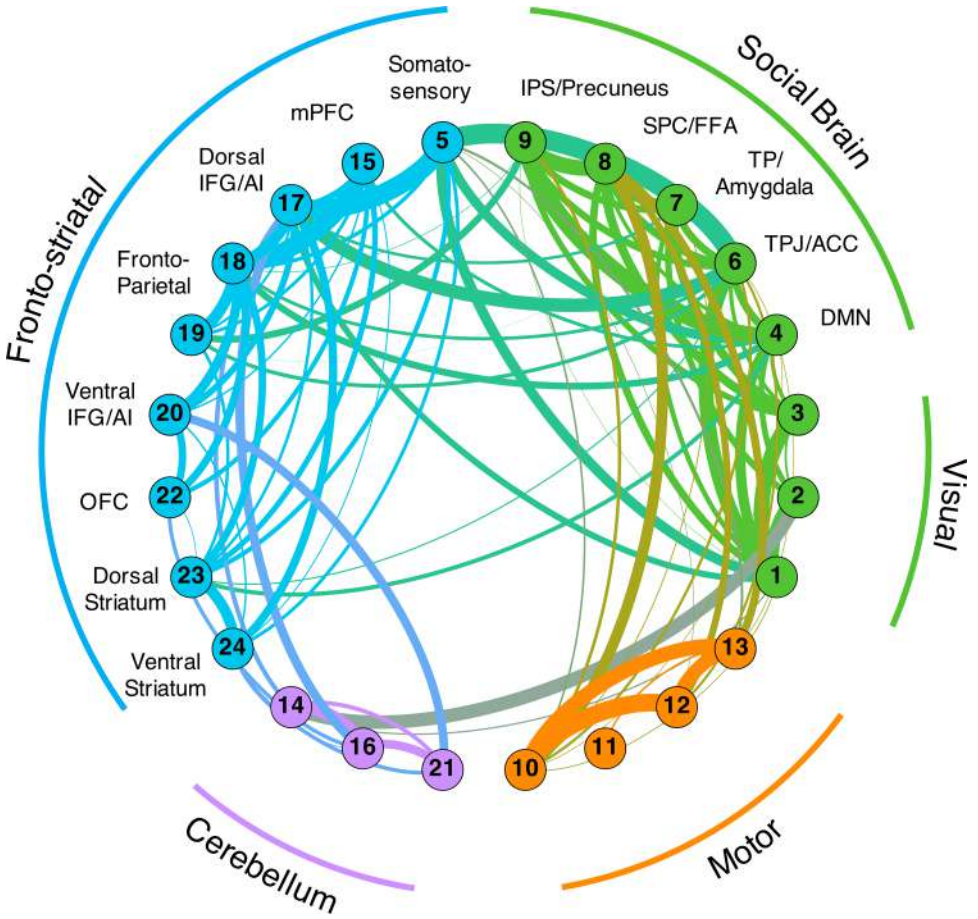

Fig. 6. Network graphs were constructed using the ROI-specific time-series from the dual regression analysis. Components were clustered together using community detection algorithms and nodal communities are indicated by separate colors. The strength of connectivity between components is indicated by the width of the edges between them. Edge colors are a blend of the node colors that they connect. We identified four broad communities: (1) a motor cluster; (2) a cerebellum cluster; (3) a fronto-striatal cluster; (4) and a cluster of components that related to the visual system and a broad collection of components related to the social brain.

transition from childhood to adolescence (Blakemore, 2008, 2012; Blakemore and Mills, 2014), we did not find significant linear or curvilinear age-related differences in any of our analyses. These findings suggest that while there are refinements in social brain regions across development, as highlighted by previously observed changes in structural and univariate functional measures (e.g. Blakemore *et al.*, 2007; Burnett *et al.*, 2009; Mills *et al.*, 2014; van den Bos *et al.*, 2011; Gweon *et al.*, 2012; Tamnes *et al.*, 2013; Van Hoorn *et al.*, 2016), the underlying functional network architecture may already be in place by late childhood. This conclusion is supported by the recovery of independent components in our task data which closely resemble those derived from resting state analyses (e.g. default mode and fronto-parietal networks; Laird *et al.*, 2011). As resting state connections are thought to reflect long-term, stable network relationships (Fox and Raichle, 2007; Wang *et al.*, 2011), their emergence in task data is perhaps unsurprising since it is unlikely that short-term, task-related organization of the brain would completely eliminate these durable networks (e.g. Gratton *et al.*, 2018). While follow-up developmental studies are necessary to replicate and extend the current work, it may be that pathways within the brain that support communication between nodes within networks emerge relatively early, whereas regional changes (e.g. grey matter features, activation) continue to be refined across longer time scales. We find tentative support for this idea by showing that there are some (albeit relatively weak) changes across age in univariate activation during the task in social brain regions. Alternatively, an adult-like social network may emerge earlier in development than other functional brain networks, given its foundational importance to human survival and development (e.g. Dunbar and Shultz, 2007). Support for this idea can be found in research showing that social cognitive regions such as the TPJ show early (e.g. by 7 months) functional organization as related to social cognition (Hyde *et al.*, 2018). Extending these findings both earlier in development and investigating how developmental trajectories of this network relates to developmental trajectories of other defined networks will be important for resolving the tension between the current findings and the body of literature showing regional changes across adolescence in the social brain.

Notably, design considerations of the present study pose some limitations and preclude our ability to rule out potential developmental effects. First, the domain of social cognition is broad and comprises processing of social-affective information, mentalizing about self and others and understanding and acting on more complex social emotions, amongst other processes (Blakemore and Mills, 2014). Future research should build on the current work by utilizing these methods to tap into different aspects of social cognition during the assessment of the social brain's functional architecture, which might show different developmental patterns. Additionally, functional

connectivity between these regions could be investigated in a task-free environment, allowing us to evaluate the functional architecture of this system at rest without the constraints of any one task design. It would also be useful for future research to explore the relationship between the social brain network and the default mode network (DMN). These two networks show significant spatial overlap. Specifically, 72% of voxels within our defined social brain network also fall within the mask of the DMN as defined by Laird and colleagues (Laird *et al*., 2011; for a discussion see Mars *et al*., 2012). However, functional connectivity patterns of regions that do not overlap (such as the amygdala and temporal pole) might serve to differentiate between these two networks. These questions will be important for future research to address.

Finally, we utilized a cross-sectional design, which, while often useful for initial questions and exploratory analyses, has been shown to be less sensitive in detecting developmental effects compared with longitudinal approaches (Kraemer *et al*., 2000; Crone and Elzinga, 2015). Utilizing repeated measures in order to examine within-person changes across the transition from childhood to adolescence could shed more light on developmental processes. In addition to the substantive question at hand, many analytic techniques utilized in the current manuscript have yet to be applied to longitudinal neural data, and as such will represent a methodological advance in our ability to further probe developmental data.

Conclusions

Taken together, the methods and findings in the current manuscript represent an important step forward in our understanding of functional relationships between regions of the social brain. Utilizing a multi-method analytic approach, we were able to show that there are strong, but not exclusive, networks between regions previously implicated in social cognition. These results highlight the need for applying methodologies consistent with our theoretical understanding of how the brain operates, namely that neural regions do not operate in isolation. Rather, the brain executes cognition and behavior across a broad network of regions that contribute computationally to ultimate outcomes. Future research should therefore start to integrate an understanding of functional connectivity to the neurodevelopmental work on the social brain, which has thus far largely focused on univariate activation. This integration not only has implications for improving our ability to propose and test more specific hypotheses of normative development (Pfeifer and Allen, 2016), but also a prime place to ask additional questions related to individual differences in network architecture and how these might relate to typical and atypical social and behavioral outcomes during development. In short, the social brain shows many characteristics of a functional network, suggesting a new framework where neuroscientists consider regions of the social brain in concert, rather than in isolation.

Supplementary data

Supplementary data are available at *SCAN* online.

Acknowledgements

Author Contributions: E.H.T. designed research; E.H.T. performed research; E.M.M. and J.V.H. analyzed data; E.M.M., J.V.H., J.R.C. and E.H.T. wrote the paper. We greatly appreciate the assistance of the Biomedical Imaging Center at the University of Illinois.

Funding

This research was supported by a grant from the National Institutes of Health (R01DA039923) and generous funds from the Department of Psychology at the University of Illinois.

Conflict of interest. None declared.

References

Adolphs, R. (2009). The social brain: neural basis of social knowledge. *Annual Review of Psychology*, **60**, 693–716.

Aristotle (1944). Aristotle in 23 Volumes, vol. 21, translated by H. Rackham. Cambridge, MA Harvard University Press; London: William Heinemann Ltd.

Beckmann, C.F., Mackay, C.E., Filippini, N., Smith, S.M. (2009). Group comparison of resting-state FMRI data using multi-subject ICA and dual regression. *NeuroImage*, **47**(Sup1), S148.

Beckmann, C.F., Smith, S.M. (2004). Probabilistic independent component analysis for functional magnetic resonance imaging. *IEEE Transactions on Medical Imaging*, **23**(2), 137–52.

Blakemore, S.J. (2008). The social brain in adolescence. *Nature Reviews Neuroscience*, **9**(4), 267–77.

Blakemore, S.J. (2012). Imaging brain development: the adolescent brain. *NeuroImage*, **61**(2), 397–406.

Blakemore, S.-J., Mills, K.L. (2014). Is adolescence a sensitive period for sociocultural processing? *Annual Review of Psychology*, **65**, 187–207.

Blakemore, S.-J., den Ouden, H., Choudhury, S., Frith, C. (2007). Adolescent development of the neural circuitry for thinking about intentions. *Social Cognitive and Affective Neuroscience*, **2**, 130–9.

Brett, M., Anton, J.L., Valabregue, R., Poline, J.B. (2002, June). Region of interest analysis using an SPM toolbox.. In *8th International Conference on Functional Mapping of the Human Brain*, (Vol. 16, No. 2, p. 497).

Brothers, L. (1990). The social brain: a project for integrating primate behavior and neurophysiology in a new domain. *Concepts Neuroscience*, **1**, 27–51.

Bullmore, E.T., Bassett, D.S. (2011). Brain graphs: graphical models of the human brain connectome. *Annual Review of Clinical Psychology*, **7**, 113–40.

Burnett, S., Bird, G., Moll, J., Frith, C., Blakemore, S.-J. (2009). Development during adolescence of the neural processing of social emotion. *Journal of Cognitive Neuroscience*, **21**, 1736–50.

Burnett, S., Blakemore, S.J. (2009). Functional connectivity during a social emotion task in adolescents and in adults. *European Journal of Neuroscience*, **29**(6), 1294–301.

Ciric, R., Wolf, D.H., Power, J.D., *et al*. (2017). Benchmarking of participant-level confound regression strategies for the control of motion artifact in studies of functional connectivity. *NeuroImage*, **154**, 174–87.

Cohen, J.R., D'Esposito, M. (2016). The segregation and integration of distinct brain networks and their relationship to cognition. *Journal of Neuroscience*, **36**(48), 12083–94.

Crone, E.A., Elzinga, B.M. (2015). Changing brains: how longitudinal functional magnetic resonance imaging studies can

inform us about cognitive and social-affective growth trajectories. *Wiley Interdisciplinary Reviews: Cognitive Science*, **6**(1), 53–63.

Decety, J., Lamm, C. (2007). The role of the right temporoparietal junction in social interaction: how low-level computational processes contribute to meta-cognition. *The Neuroscientist*, **13**(6), 580–93.

Dufour, N., Redcay, E., Young, L., Mavros, P.L., Moran, J.M., Triantafyllou, C., Gabrieli, J.D.E., Saxe, R. (2013). Similar brain activation during false belief tasks in a large sample of adults with and without autism. *PloS One*, **8**(9), e75468.

Dunbar, R.I., Shultz, S. (2007). Evolution in the social brain. *Science*, **317**(5843), 1344–7.

Eickhoff, S.B., Stephan, K.E., Mohlberg, H., Grefkes, C., Fink, G.R., Amunts, K., Zilles, K. (2005). A new SPM toolbox for combining probabilistic cytoarchitectonic maps and functional imaging data. *NeuroImage*, **25**(5843), 1325–35.

Egger, H.L., Pine, D.S., Nelson, E., *et al.* (2011). The NIMH Child Emotional Faces Picture Set (NIMH-ChEFS): a new set of children's facial emotion stimuli. *International Journal of Methods in Psychiatric Research*, **20**(3), 145–56.

Filippini, N., MacIntosh, B.J., Hough, M.G., *et al.* (2009). Distinct patterns of brain activity in young carriers of the APOE-ε4 allele. *Proceedings of the National Academy of Sciences*, **106**(17), 7209–14.

Fox, M.D., Raichle, M.E. (2007). Spontaneous fluctuations in brain activity observed with functional magnetic resonance imaging. *Nature Reviews Neuroscience*, **8**(9), 700.

Frith, C.D., Frith, U. (2007). Social cognition in humans. *Current Biology*, **17**(16), R724–32.

Gratton, C., Laumann, T.O., Nielsen, A.N., *et al.* (2018). Functional brain networks are dominated by stable group and individual factors, not cognitive or daily variation. *Neuron*, **98**(2), 439–52.

Gweon, H., Dodell-Feder, D., Bedny, M., Saxe, R. (2012). Theory of mind performance in children correlates with functional specialization of a brain region for thinking about thoughts. *Child Development*, **83**(6), 1853–68.

Hyde, D.C., Simon, C.E., Nikolaeva, J.I., Ting, F. (2018). Functional organization for theory of mind in pre-verbal infants: a near-infrared spectroscopy study. *The Journal of Neuroscience*, **38**(18), 4264–74.

Kraemer, H.C., Yesavage, J.A., Taylor, J.L., Kupfer, D. (2000). How can we learn about developmental processes from cross-sectional studies, or can we? *American Journal of Psychiatry*, **157**(2), 163–71.

Laird, A.R., Fox, P.M., Eickhoff, S.B., *et al.* (2011). Behavioral interpretations of intrinsic connectivity networks. *Journal of Cognitive Neuroscience*, **23**(12), 4022–37.

Lancichinetti, A., Fortunato, S. (2012). Consensus clustering in complex networks. *Scientific Reports*, **2**, 336.

Lieberman, M.D. (2007). Social cognitive neuroscience: a review of core processes. *Annual Review of Psychology*, **58**, 259–89.

Mars, R.B., Neubert, F.X., Noonan, M.P., Sallet, J., Toni, I., Rushworth, M.F. (2012). On the relationship between the "default mode network" and the "social brain". *Frontiers in Human Neuroscience*, **6**, 189.

McLaren, D.G., Ries, M.L., Xu, G., Johnson, S.C. (2012). A generalized form of context-dependent psychophysiological interactions (gPPI): a comparison to standard approaches. *NeuroImage*, **61**(4), 1277–86.

Mills, K.L., Lalonde, F., Clasen, L., Giedd, J.N., Blakemore, S.-J. (2014). Developmental changes in the structure of the social brain in late childhood and adolescence. *Social Cognitive and Affective Neuroscience*, **9**, 123–31.

Nelson, E.E., Jarcho, J.M., Guyer, A.E. (2016). Social re-orientation and brain development: an expanded and updated view. *Developmental Cognitive Neuroscience*, **17**, 118–27.

Nelson, E.E., Leibenluft, E., McClure, E.B., Pine, D.S. (2005). The social re-orientation of adolescence: a neuroscience perspective on the process and its relation to psychopathology. *Psychological Medicine*, **35**(2), 163–74.

Pfeifer, J.H., Allen, N.B. (2012). Arrested development? Reconsidering dual-systems models of brain function in adolescence and disorders. *Trends in Cognitive Sciences*, **16**(6), 322–29.

Pfeifer, J.H., Masten, C.L., Borofsky, L.A., Dapretto, M., Fuligni, A.J., Lieberman, M.D. (2005). Neural correlates of direct and reflected self-appraisals in adolescents and adults: when social perspective-taking informs self-perception. *Child Development*, **80**(4), 1016–38.

Power, J.D., Cohen, A.L., Nelson, S.M., *et al.* (2011). Functional network organization of the human brain. *Neuron*, **72**(4), 665–78.

Power, J.D., Barnes, K.A., Snyder, A.Z., Schlaggar, B.L., Petersen, S.E. (2012). Spurious but systematic correlations in functional connectivity MRI networks arise from subject motion. *NeuroImage*, **59**(3), 2142–54.

Qu, Y., Galvan, A., Fuligni, A.J., Lieberman, M.D., Telzer, E.H. (2015). Longitudinal changes in prefrontal cortex activation underlie declines in adolescent risk taking. *Journal of Neuroscience*, **35**, 11308–14.

Rissman, J., Gazzaley, A., D'esposito, M. (2004). Measuring functional connectivity during distinct stages of a cognitive task. *NeuroImage*, **23**(2), 752–63.

Rubinov, M., Sporns, O. (2010). Complex network measures of brain connectivity: uses and interpretations. *NeuroImage*, **52**(3), 1059–69.

Rubinov, M., Sporns, O. (2011). Weight-conserving characterization of complex functional brain networks. *NeuroImage*, **56**(4), 2068–79.

Saxe, R. (2006). Uniquely human social cognition. *Current Opinion in Neurobiology*, **16**(2), 235–9.

Schurz, M., Radua, J., Aichhorn, M., Richlan, F., Perner, J. (2014). Fractionating theory of mind: a meta-analysis of functional brain imaging studies. *Neuroscience & Biobehavioral Reviews*, **42**,9–34.

Somerville, L.H. (2013). The teenage brain: sensitivity to social evaluation. *Current Directions in Psychological Science*, **22**(2), 121–7.

Somerville, L.H., Jones, R.M., Ruberry, E.J., Dyke, J.P., Glover, G., Casey, B.J. (2013). The medial prefrontal cortex and the emergence of self-conscious emotion in adolescence. *Psychological science*, **24**(8), 1554–62.

Smith, S.M., Hyvärinen, A., Varoquaux, G., Miller, K.L., Beckmann, C.F. (2014). Group-PCA for very large fMRI datasets. *NeuroImage*, **101**,738–49.

Tamnes, C.K., Walhovd, K.B., Dale, A.M., *et al.* (2013). Brain development and aging: overlapping and unique patterns of change. *NeuroImage*, **68**, 63–74.

Tohka, J., Foerde, K., Aron, A.R., Tom, S.M., Toga, A.W., Poldrack, R.A. (2008). Automatic independent component labeling for artifact removal in fMRI. *NeuroImage*, **39**(3), 1227–45.

van den Bos, W., van Dijk, E., Westenberg, M., Rombouts, S.A., Crone, E.A. (2011). Changing brains, changing perspectives: the neurocognitive development of reciprocity. *Psychological Science*, **22**(1), 60–70.

Van Dijk, K.R., Sabuncu, M.R., Buckner, R.L. (2012). The influence of head motion on intrinsic functional connectivity MRI. *NeuroImage*, **59**(1), 431–8.

van Hoorn, J., Van Dijk, E., Güroğlu, B., Crone, E.A. (2016). Neural correlates of prosocial peer influence on public goods game donations during adolescence. *Social Cognitive and Affective Neuroscience*, **11**(6), 923–33.

van Overwalle, F. (2009). Social cognition and the brain: a meta-analysis. *Human Brain Mapping*, **30**(3), 829–58.

Wang, J.H., Zuo, X.N., Gohel, S., Milham, M.P., Biswal, B.B., He, Y. (2011). Graph theoretical analysis of functional brain networks: test-retest evaluation on short-and long-term resting-state functional MRI data. *PloS One*, **6**(7), e21976.